Dynamics in between Structural and Electrical Properties of as Grown ZnO Thin Films by Thermal ALD

Bilge İMER[1]* (iD)

[1]Middle East Technical University, Metallurgical and Materials Engineering, Ankara, Turkey

Graphical/Tabular Abstract (Grafik Özet)

Structural and stoichiometric defects play a crucial role in determining the electrical properties of ZnO, and are strongly controlled by the growth method and conditions. In this study, the dynamics between structural and electrical properties for various ALD growth conditions were analyzed to identify the main contributors to n-type conductivity. / Yapısal ve stokiyometrik kusurlar, ZnO'nun elektriksel özelliklerinin belirlenmesinde çok önemli bir rol oynar. Bu kusurlar ancak büyüme yöntemi ve koşulları ile kontrol edilebilir. Bu çalışmada çeşitli ALD büyüme koşulları için yapısal ve elektriksel özellikler arasında dinamikler, n-tipi iletkenliği etkileyen ana faktörleri belirlemek amacı ile analiz edildi.
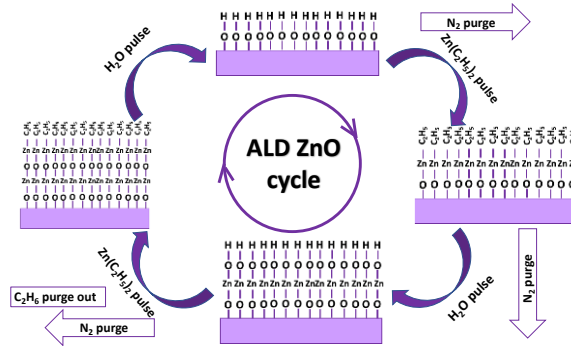
Figure A: Representation of ZnO growth cycle by ALD

/**Şekil A:**.Temsili ALD ile ZnO büyütme döngüsü

Highlights (Önemli noktalar)

➢ Temperature and relative DEZ and DI pulse times were the strongest influencers of ZnO structural and ,hence, the electrical properties./Büyüme sıcaklığı ve göreceli DEZ&DI atış süreleri ZnO'nun yapısal ve dollayısıyla elektriksel özelliklerini en çok etkilyen büyütme faktörleridir.

➢ The contribution of hydrogen impurities, zinc interstitials and oxygen vacancies to resistivity values were observed experimentally./ Hidrojen safsızlıkjlarının, çinko arayerlerinin ve oksijen boşluklarının direnç değerlerine katkısı deneysel olarak gözlemlenmiştir.

➢ The strongest correlation was observed in between hydrogen impurity concentration and resistivity for various growth conditions./ En güçlü korelasyon, çeşitli büyüme koşulları için hidrojen safsızlık konsantrasyonu ile direnç arasında gözlendi.

Aim (Amaç): The main purpose of this study was to identify the specific defect/impurity contributors to n-type electrical conductivity in different growth conditions for ALD grown ZnO films. / Bu çalışmanın temel amacı, ALD ile büyütülmüş ZnO filmleri için farklı büyüme koşullarında n-tipi elektrik iletkenliğine katkıda bulunan spesifik kusurları/safsızlıkları tanımlamaktı.

Originality (Özgünlük): An experimental evidence is presented for defect/impurity concentration, especially hydrogen impurity, contribution to n-type conductivity in ZnO. / ZnO n-tipi iletkenliğine kusur ve safsızlıkların, özellikle hidrojen safsızlıklarını,n katkı sağlayan mekanizma olduğunun kanıtı deneysel olarak sunulmuştur.

Results (Bulgular):

The contribution of hydrogen impurities, zinc interstitials and oxygen vacancies to conductivity was observed at different growth conditions. Lowest resistivity and highest average % transmittance were obtained as 6.8×10^{-3} ohm.cm and 92% in visible spectrum (380-700 nm), respectively.

Conclusion (Sonuç): Main defect/impurity contributors to n-type conductivity in ZnO were experimentally identified. / ZnO n-tipi iletkenliğine başlıca kusurların/safsızlıkların katkısı deneysel olarak ortaya konulmuştur.

---

*Corresponding author, e-mail: bimer@metu.edu.tr

Dynamics in between Structural and Electrical Properties of as Grown ZnO Thin Films by Thermal ALD

Bilge İMER[1]* ⓘD

[1]Middle East Technical University, Metallurgical and Materials Engineering, Ankara, Turkey

Abstract

The mechanism behind n-type conductivity of undoped ZnO films are not understood well. One and two dimensional defects (grain boundaries, dislocations), and zero dimensional stoichiometric point defects (vacancies, self-interstitials and impurities) play a crucial role in determining the electrical properties of ZnO. All defect mechanisms are strongly controlled by the growth method and conditions. While it is more straightforward examining the one and two dimensional defects, measuring and unveiling the mechanism behind the zero dimensional point defect contribution and their sole effect on the electrical properties are challenging. This is why there has been controversial discussion of results among experimental and computational works relating physical and chemical properties of ZnO to sustainable electrical properties. In this study, to correlate the dynamics in between structural and electrical properties of ZnO grown by thermal atomic layer deposition (ALD); growth temperature, DEZ and DI water precursor pulse times, DEZ/DI water precursor pulse ratio, and N_2 purge time were varied. To obtain growth condition specific structural and electrical properties; XRD, AFM, profilometer, ellipsometry, XPS/CasaXPS, UV-VIS spectrometer, Hall-Effect measurements were utilized. Although, there was no strong correlation for oxygen vacancies, the contribution of hydrogen impurities, zinc interstitials and oxygen vacancies to conductivity was observed at different growth conditions. Lowest resistivity and highest average % transmittance were obtained as 6.8×10^{-3} ohm.cm and 92% in visible spectrum (380-700 nm), respectively.

Termal ALD ile Büyütülmüş ZnO İnce Filmlerin Yapısal ve Elektriksel Özellikleri Arasındaki Dinamikler

Öz

Katkısız ZnO filmlerin n-tipi iletkenliğinin ardındaki mekanizma iyi anlaşılmamıştır. 1 ve 2 boyutlu kusurlar (tane sınırları, dislokasyonlar) ve 0 boyutlu stokiyometrik nokta kusurları (boşluklar, kendi arayerleri ve safsızlıklar), ZnO'nun elektriksel özelliklerinin belirlenmesinde çok önemli bir rol oynar. Bu kusur mekanizmaları büyüme yöntemi ve koşulları tarafından güçlü bir şekilde kontrol edilir. 1 ve 2 boyutlu kusurları karakterize etmek ve incelemek daha basit olsa da, 0 boyutlu nokta kusur katkısının arkasındaki mekanizmayı ve bunların elektriksel özellikler üzerindeki tek etkisini ölçmek ve ortaya çıkarmak zorlayıcıdır. ZnO'nun fiziksel ve kimyasal özellikleri ile elektriksel özellikleri arasında ilişki kuran deneysel ve hesaplamalı çalışmalar arasında tartışmalı sonuçların bulunmasının nedeni de budur. Bu çalışmada, termal ALD ile büyütülen ZnO'nun yapısal ve elektriksel özellikleri arasındaki dinamikleri ilişkilendirmek amacıyla; büyüme sıcaklığı, DEZ ve DI öncü atım süreleri, DEZ/DI öncü atım oranı ve N2 temizleme süresi değiştirildi. Büyüme durumuna özgü yapısal ve elektriksel özellikleri elde etmek için; XRD, AFM, profilometre, elipsometri, XPS/CasaXPS, UV-VIS spektrometresi, Hall-Effect ölçümlerinden yararlanılmıştır. Oksijen boşlukları için güçlü bir korelasyon olmamasına rağmen, farklı büyüme koşullarında hidrojen safsızlıklarının, çinko ara katmanlarının ve oksijen boşluklarının iletkenliğe katkısı gözlemlendi. Görünür spektrumda (380-700 nm) en yüksek ortalama % geçirgenlik %92 olarak ve en düşük özdirenç 6,8×10⁻³ ohm.cm olarak elde edilmiştir.

1. INTRODUCTION (GİRİŞ)

In recent years, Al_2O_3, ZnO, SnO_2, ITO, AZO, FZO, FTO have been the most common metal oxides studied and used for wide range of applications [1-5]. Among all, zinc oxide (ZnO) distinguishes itself from other metal oxides for being abundant, available, cheap and non-toxic. Also, its high

thermal conductivity [6], high electron mobility [7], high radiation hardness [8], direct and wide bandgap [9], high free-exciton binding energy [10], surface chemical reactivity, and large piezoelectric constants [11], makes it an ideal material choice for various applications.

ZnO is an innate n-type II-VI semiconductor material with covalent and ionic bonding characteristics. ZnO can exist in hexagonal wurtzite, zincblend and rocksalt crystal structure forms. While wurtzite structure is thermodynamically preferred at ambient conditions, it can be transformed into rocksalt structure under high pressure conditions. Metastable zincblend phase can be obtained when grown over zincblend substrates or it appears in wurtzite structure seperated by defects when grown over highly lattice mismatched substrates. [7] ZnO's most stable crystal form, wurtzite, is the same as GaN, but, unlike GaN, ZnO is available in large bulk size single crystals [10]. However, due to uncontrollable electrical properties, the use of ZnO has been limited in semiconductor industry.

The similarity in between ZnO and GaN is not only limited by their crystal structures. ZnO (3.37 eV) has very similar direct wide bandgap as GaN (3.4 eV), except with larger exciton binding energy (60 meV for ZnO vs. 25 meV for GaN) yielding a more stable and higher emission efficiency at room temperature and above [12]. ZnO has been studied to complement GaN, providing substrate with its large available crystal size [13] and functional interlayers integrated in nitride device structures, or to substitute GaN's function. Large exciton binding energies make ZnO a better candidate for UV/blue light emitting applications (like LEDs and lasers). However, it has been a challenge to achieve p-type doping due to its high unintentional n-type innate doping characteristics originated mostly from its structural and point defects [14]. Due to its wide bandgap, ZnO is transparent to visible spectrum. Therefore, it can be utilized as transparent contact (TCO) to any light emitting devices (diodes and displays) [15-16], light collecting devices (like solar cells, detectors) [17], or to touch screens/energy saving windows. Another application area is its use in transistors [18-19] as conducting channel. Its high radiation hardness against MeV proton irradiation levels, makes ZnO a good candidate for space applications. Another property of ZnO is its spontaneous polarization along c-axis in wurtzite structure; this built-in field can be utilized in acoustic wave and piezoelectric devices [20-21].

Different methods like MOCVD [21], MBE [22], PLD [23], sputtering [24], ALD [5] have been employed to grow ZnO films. ALD has many advantages over the aforementioned alternative growth methods. Due to its low processing temperatures, large area uniformity and high conformal coverage, it is economical, applicable over low melting temperature materials like polymers and textile, and compatible with large area industrial applications and 3D device architectures; precise thickness control is achievable with atomically smooth interfaces; and it is easily integrable to other semiconductor processes.

Although, ZnO has many potential application areas, i) controlling and reproducibility of n-type ZnO's electrical properties, and ii) achieving p-type

Table 1. Density functional calculations summary for defects and H impurities in n-type as grown

ZnO [25] (n-tipi ZnO filmlerde kusurlar ve H safsızlıkları yoğunluk fonksiyonel hesaplamaları özeti)

Defect/Impurity	Formation Energy	Defect Transition Level	Carrier Type	Notes type
V_O	Low	Deep	**Donor**	Acts as compensator in p type ZnO
V_{Zn}	Low	Deep	Acceptor	Acts as compensator in n type ZnO
O_i^t	High	Neutral	NA	Oxygen interstitial in tetrahedral sites
O_i^o	High	Deep	Acceptor	Oxygen interstitial in octahedral sites
Zn_i	Mid	Shallow	**Donor**	More stable in octahedral sites, diffuse out easily
O_{Zn}	High	Deep	Acceptor	Large off-site displacement, not many
Zn_O	Mid	Shallow	**Donor**	Large off-site displacement
H_i	Low	Shallow	**Donor**	Forms bond with ZnO as ZnOH Highly mobile, diffuse out easily
H_O	Low	Shallow	**Donor**	More stable than interstitial H

ZnO remain as a challenge. Therefore, understanding the role of defects/impurities, growth variables and material property dynamics are indispensible for creating reproducible and sustainable ZnO films for electronic applications.

Structural defects and stoichiometric point defects play a crucial role in determining the electrical properties of ZnO. The main stoichiometric point defects that is considered to exist in ZnO are: Zn vacancies (V_{Zn}), O vacancies (V_O), Zinc interstitials (Zn_i), Oxygen interstitals (O_i), Zinc antisites (Zn_O), Oxygen antisites (O_{Zn}), and substitutional or interstitial impurities like hydrogen or carbon. The summary of defects and impurities present in as grown ZnO is summarized in Table 1. If all of these defects were energetically favored to exist, V_O, Zn_i, Zn_O would act like a donor, and V_{Zn}, O_i and O_{Zn} act like an acceptor. Zn rich growth regime favors donors (V_O, Zn_i, Zn_O), and O rich growth conditions support the existence of acceptors (V_{Zn}, O_i and O_{Zn}). But not all these defects are energetically favored to exist. Even when they are favored to exist not all would participate in n- or p-type conductivity. Based on computational results from density functional theory (DFT) demonstrated; V_O and V_{Zn} are the lowest energy, Zn_i and Zn_O next highest, then lastly followed by O_i and O_{Zn} with highest formation energies [25].

Oxygen vacancies (V_O), with lowest formation energy, are expected to form readily. However, it was calculated these defects are deep state donors and can not add to n-type conductivity but they compensate p-type carriers. Zinc vacancies (V_{Zn}) has the lowest formation energy among all point defects, and they are deep state acceptors. Therefore, they only act like n-type compensator. Zinc interstitials (Zn_i) prefers the octahedral sites. They and zinc antisites (Zn_O) are shallow donors, can participate in n-type conduction event, however, have relatively higher formation energies and unstable. Oxygen interstitials (O_i) and and antisites (O_{Zn}) are both inactive or deep acceptors and have the highest calculated formation energies. They do not exist in significant amount [26-30].

Theoretically, undoped ZnO exist as unintentionally n-type doped. Among all stoichiometric defects only Zn_i and V_O can be the reason for it. However, as mentioned, calculated V_O donor levels are deep, can not be ionized, and Zn_i have relatively high formation energies.Therefore, hydrogen (H) impurity was suggested to be the source for n-type conductivity in ZnO. H behaves amphoteric in almost all semiconductors, i.e. acts as positive charge in p-type and as negative charge in n-type.. But based on density functional calculations, H acts as a shallow n-type donor in ZnO, and have a low formation energy. Also, H is the smallest atom in periodic table and can easily diffuse into ZnO lattice. In addition, H exist in all growth environments. Interstitial H binds to oxygen atom in ZnO forming $Zn(OH)_2$ [7, 31]. Experimental results do not always agree with the theoretical calculations. For example, with calculated formation energy of 3.9 eV for oxygen vacancies, the concentration of V_O is implied to be on the order of 10^8 cm^{-3} while the experimental value is in the range of 10^{17} to 10^{19} cm^{-3}. The debate on what contributes to ZnO n-type conductivity still exists. [32-35]

Either the H impurities or O vacancies, etc., all of the point defect/impurity presence can be strongly controlled by the growth type and growth conditions. To obtain reproducable conductivities for ZnO, the mechanism and its relation with structural property should be addressed well. Within the scope of this study, after relating processing conditions with ZnO's structural properties, the electrical properties are correlated with structural properties and growth variables to shed light on the n-type conductivity mechanism. A special attention was paid on analyzing the presence of mentioned defects and their correlation with resistivity.

2. MATERIALS AND METHODS (MATERYAL VE METOD)

2.1. Experimental Design (Deney Tasarımı)

Both (100) silicon and quartz were used as substrates to deposit ZnO films. Substrates were cleaned with acetone, isopropyl alcholol DI water in US bath prior to growth. Silicon substrates were dipped into HF:DI (1:10) to remove the natural oxide. ZnO films were deposited by OkyayTech thermal atomic layer deposition (ALD). Diethylzinc (DEZ-$Zn(C_2H_5)_2$, (Sigma Aldrich) was used as Zn precursor and deionized water (DI) was used as oxygen source. Both precursors were kept at room temperature. Nitrogen (≥99.99%) was utilized as a carrier gas with 20 sccm flow rate. The chamber base pressure was kept at 640 µbar. The ZnO thin films were optimized by changing growth temperature (between 125- 200º C), DEZ and DI pulse times (as 15, 50, 100 ms) at DEZ/DI ratio of 1, DEZ/DI ratio (from 0.25 to 2), and nitrogen purge time (as 2, 5, and 10s) as summarized in Table 2.

Table 2. Experimental parameters (Deneysel parametreler)

Sample #	Temperature (°C)	Cycle	DEZ Pulse (ms)	DI Pulse (ms)	DEZ/DI Ratio	Purge time (s)
1	200	400	15	15	1	10
2	175	400	15	15	1	10
3	150	400	15	15	1	10
4	125	400	15	15	1	10
5	175	400	100	100	1	10
6	175	400	50	50	1	10
7	175	400	50	50	1	5
8	175	400	50	50	1	2
9	175	400	50	100	2	10
10	175	400	100	50	0.5	10
11	175	400	200	50	0.25	10

The number of ALD growth cycle was kept at 400 cycles for all growth conditions yielding 70-90 nm thickness variation for all conditions.

The process optimization parameters were set into four groups. The temperature variation was identifed as **Group 1**; the variation in DEZ and DI pulse times was identified as **Group 2**; the change in purge time was named as **Group 3**; and the change in DEZ/DI ratio was identified as **Group 4**. Each group variable change was correlated with structural properties (thickness-growth rate, crystal quality, surface roughness, stoichiometry), and with electrical (resistivity, carrier density and mobility) and optically%transmittance in visible range to analyze the impact of various ALD growth conditions on potential electrical and optical application performance.

2.2. Characterization (Karakterizasyon)

dimensions. In Figure 2, the dimensions of the workpiece and tool, and the processing principle are shown. The experiments were carried out on the Furkan compact 1 Z-NC type die-sinking electro erosion bench. Belone EDM F liquid with high flash point and low viscosity was used as dielectric fluid.

The film thicknesses were determined using V-VASE spectroscopic ellipsometer and Dektak-8 surface profiler. Surface roughness values were measured utilizing Veeco MultiMode V atomic force microscopy (AFM) in tapping mode. The 2θ scans in between 30-70° were taken with Rigaku Ultima IV X-ray Diffraction (XRD) (Cu-Ka radiation with a wavelength of λ= 1.5406 Å) operated at 40 kV and 40 mA. The electrical and optical characterizations were carried out with

samples grown on quartz substrates; structural characterization were done on silicon substrates. The transmission values of all samples were analyzed with Cary 100 UV-VIS Spectrometer in between 300-700 nm wavelength range. ZnO stoichiometry and binding energies were measured with Phi5000 Versa Probe X-Ray Photoelectron Spectroscopy (XPS). CasaXPS software was used to analyze binding energies. The resistivity, carrier density and mobility values were characterized by ECOPIA HMS-3000 Hall Effect system using Van der Pauw patterns. All characterizations were carried out at room temperature.

3. RESULTS (BULGULAR)

3.1. Structural and Chemical Properties (Yapısal ve Kimyasal Özellikler)

Thickness, Growth Rate and Surface Properties

(Kalınlık, büyüme hızı ve yüzey özellikleri)

There is an optimum growth window in which the surface is saturated and all precursors used effectively to obtain a better quality film [36-40]. As summarized in Table 3, growth rates on Si substrate (2-2.31 Å/cycle) were higher than growth rates on quartz substrates (1.6-2.1 Å/cycle) due to higher thermal conductivity of Si substrates. A better fit was obtained with the ellipsometry measurements for the thickness values taken from ZnO films with underlying quartz substrates, therefore, growth rate discussions can be carried over the quartz substrate data. With increasing growth temperature, the growth rate on quartz substrates reaches to maximum value of 2.84 Å/cycle at 175°C, as the ethyl ligands were effectively removed by water with increasing temperature, then it starts to drop

again with increased desorption rates. Therefore, ALD growth window for ZnO was determined to be approximately 140°C-180°C. When discussing structural and chemical properties this window will be utilized for further analysis.

Table 3. Summary of thickness, growth rate and surface roughness values (Kalınlık, büyüme hızı ve yüzey pürüzlülüğü değerlerinin özeti)

	Sample #	Variable sets	Variable	Surface Roughness (Rms) for 1 ∞m^2 area (nm)	Thickness over Si (nm)	Growth Rate over Si (A/cycle)	Thickness over Quartz (nm)	Growth Rate over Quartz (A/cycle)
GROUP 1	1	Increasing Temperature	200°C	2.62	84	2.1	73.61	1.84
	2		175°C	1.4	92.3	2.31	75.27	1.88
	3		150°C	1.82	85.9	2.15	73.45	1.84
	4		125°C	2.87	79.8	2	64.3	1.6
GROUP 2	5	Increasing DEZ & DI Pulse Time	100 ms	1.91	85.4	2.13	78.08	2
	6		50 ms	1.66	85.9	2.22	78.01	2
	2		15 ms	1.4	92.3	2.31	75.27	1.88
GROUP 3	6	Increasing Purge Time	10 s	1.66	85.9	2.22	78.01	2
	7		5 s	1.95	89	2.22	80	2
	8		2 s	2.82	85	2.12	82.1	2.1
GROUP 4	9	Increasing DEZ/DI Ratio	2	1.8	90.26	2.25	79.75	2
	5		1	1.91	85.4	2.13	78.08	2
	10		0.5	2.29	82.38	2.06	78.78	1.97
	11		0.25	2.73	87.24	2.18	78.65	1.97

Table 4. Summary of XRD results for (100) and (002) peaks, and calculated average grain size for (100) and (200) reflections ((100) ve (002) pikleri XRD sonuçları ve (100) ve (002) pikleri için hesaplanmış ortalama tane bütüklükleri)

	Sample #	Variable sets	Variable	Surface Roughness (Rms) for 1 ∞m^2 area (nm)	Thickness over Si (nm)	Growth Rate over Si (A/cycle)	Thickness over Quartz (nm)	Growth Rate over Quartz (A/cycle)
GROUP 1	1	Increasing Temperature	200°C	2.62	84	2.1	73.61	1.84
	2		175°C	1.4	92.3	2.31	75.27	1.88
	3		150°C	1.82	85.9	2.15	73.45	1.84
	4		125°C	2.87	79.8	2	64.3	1.6
GROUP 2	5	Increasing DEZ & DI Pulse Time	100 ms	1.91	85.4	2.13	78.08	2
	6		50 ms	1.66	85.9	2.15	78.01	2
	2		15 ms	1.4	92.3	2.31	75.27	1.88
GROUP 3	6	Increasing Purge Time	10 s	1.66	85.9	2.15	78.01	1.95
	7		5 s	1.95	89	2.22	80	2
	8		2 s	2.82	85	2.12	82.1	2.1
GROUP 4	9	Increasing DEZ/DI Ratio	2	1.8	90.26	2.25	79.75	2
	5		1	1.91	85.4	2.13	78.08	1.95
	10		0.5	2.29	82.38	2.06	78.78	1.97
	11		0.25	2.73	82.24	2.05	78.65	1.97

As expected, the growth rate was stabilized at 2 Å/cycle for varying precursors pulse time lengths after 50 ms. For shorter pulse times, it is most likely that the surface saturation time was not sufficient. The purge time did not have any observable influence on the growth rate, just an insignificant drop most likely due to desorption of species under longer purge times. Meanwhile for DEZ/DI pulse time ratio of 1 and above, the maximum growth rate was achieved and stabilized at 2 Å/cycle. For lower DEZ/DI pulse time ratio the growth rate was lower due to insufficient DEZ pulse duration. Surface roughness rms values were in the range of 1.4-2.87 nm for 1 μm x 1 μm area. As will be discussed in

detail along with XRD results in the "Crystallinity" section, the surface roughness is a strong function of the surface precursor dynamics and growth modes (the preferred polycrystalline orientations).

Crystallinity (Kristalinite)

The final film quality is determined by the surface reaction dynamics and these reaction dynamics are highly growth temperature dependent. For ALD ZnO growth utilizing DEZ and DI water, there are 3 gorwth zones:

Zone 1: Up to around 120°C. The temperature is not high enough to get over the energy barrier to remove the ethyl-ligands with water, monoethyl zinc (MEZ) groups supersaturates the surface. Ligands prefer to attach to lowest energy surface sites, which is (002) [41]. So (002) oriented growth dominates other orientations. The ethyl ligands persists on the surface so the growth rate is low, but it increases with increasing temperature.

Zone 2: Around 120°C to around 180°C. This is the so-called ALD growth window. The growth rate becomes constant at self-limiting rate. (002) peaks are suppressed and (001) are mixed more dominantly. Due to built-in polarity of ZnO wurtzite crystal along <0001>, (002) surface can be charged positively when Zn atoms terminated and charged negatively when O atoms terminated after each cycle [39]. These highly charged surfaces are not favored for ligand exchanges suppressing (002) oriented growth and enhancing (001) oriented growth. The prematurely dissociated ethyl anion fragments saturates (002) positive Zn polar surfaces and suppresses its growth, while (100) orientation growth relatively enhenced.

Zone 3: Above 180°C. The reactants either desorbs from the surface (mainly DEZn). Growth rate decreases with increasing temperature. The positive or negative anions saturating (002) polar surfaces and suppressing its growth, break down further creating a charge neutral surface, not blocking (002) growth anymore. Therefore enhencing (002) oriented growth along c-axis. The more Zn rich (oxygen defficient) growth higher the stability of (002) orientation.

Due to growth temperature range (125°C-200°C) used in experiment sets, the growth mechanisms are Zone 2 and Zone 3 dominated. Based on XRD, AFM and ellipsometry results the zone ranges are determined to understand the surface reaction

dynamics leading to specific defect/impurity composition and finally related to electrical properties. Table 4 summarizes the XRD (100) and (200) orientation results for different growth variable sets. From these XRD results, average grain sizes for (100) and (002) orientations were calculated utilizing Debye Scherrer relation.

In Figure 1, 2θ scans show the preferred orientations of polycrystalline ZnO films. The first peak at 31.8° belongs to (100) plane perpendicular to nonpolar orientation of ZnO wurtzite cell, the second peak is the (002) plane perpendicular to main c-axis polar orientation at around 34.7°. These are the main peaks that demonstrates the preferred growth orientation of ZnO films based on growth conditions. ZnO polycrystalls have mixed orientations of (100) and (002). Relative amounts of each orientation is determined based on relative peak intensities and FWHM values.

As can be seen on Figure 1.a, With increasing growth temperature, (002) peak dominates (100) peak. The growth orientation (002) is preferred due to altered surface dynamics forming Zn rich ZnO films with increased growth temperature.

Growth temperature is the most important parameter determining the final film quality and preferred crystal orientation as described Zone 1, 2 and 3. So, in tune with XRD data, at 125°C (001) orientation was preferred, while still some (002) crystallites were aligned along c-[0001] growth direction. In Figure 2.a AFM topography image, it is possible to see fewer columnar grains aligned along growth direction. These irregular (002) plane ondulations in combined with (100) plane growth creates relatively rougher surface. As temperature increases to 200°C, c-[0001] direction growth perpendicular to (002) planes dominates more, creating a balanced mixture between (100) and (002) planes. As a result, the surface roughness values diminishes as the temperature goes up to 175°C. Above 175°C, the surface species starts to desorp creating relatively rougher surface. The AFM surface topography images show the granular surface nature due to columnar growth in preferred direction. At 125°C the surface roughness is the highest (2.87 nm), and decreases to 1.82 nm at 150°C and to 1.4 nm at 175°C as bimodal orientation distribution averages out to smoother surface features. Then at 200°C, surface desorption dynamics caused 2.62 nm surface roughness valu
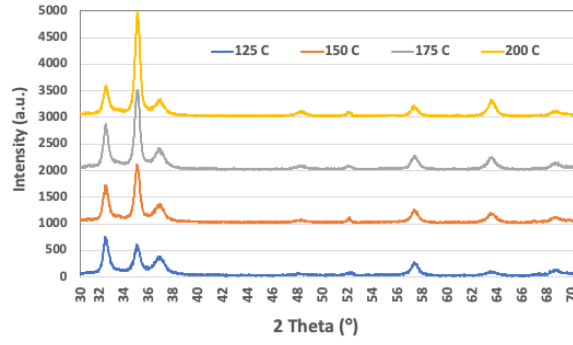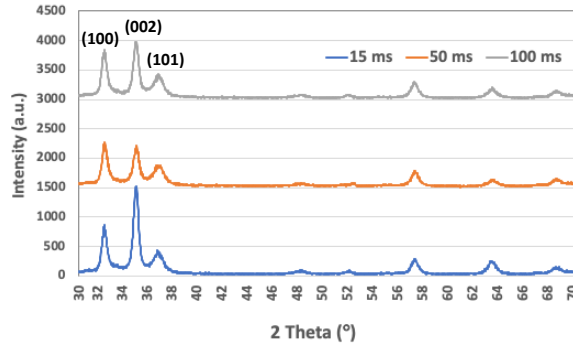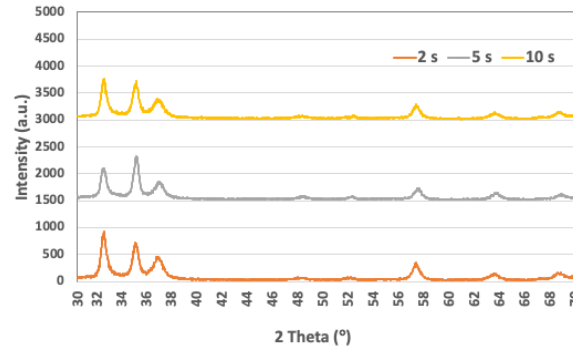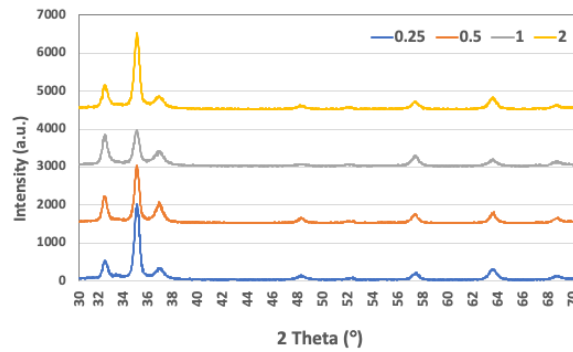
Figure 1. XRD spectrum of ZnO films for changing: **a)**growth temperature (Group 1), **b)**DEZ and DI pulse times for constant DEZ/DI ratio of 1 (Group 2), **c)**nitrogen purge time (Group 3), and **d)**DEZ/DI ratio (Group 4). (Representative peak positions are given in **b)**)(ZnO filmlerin XRD spektrumları a) büyüme sıcaklığı, b) DEZ ve DI atım süreleri, c) nitrojen temizleme süresi, ve d) DEZ/DI oranına göre)
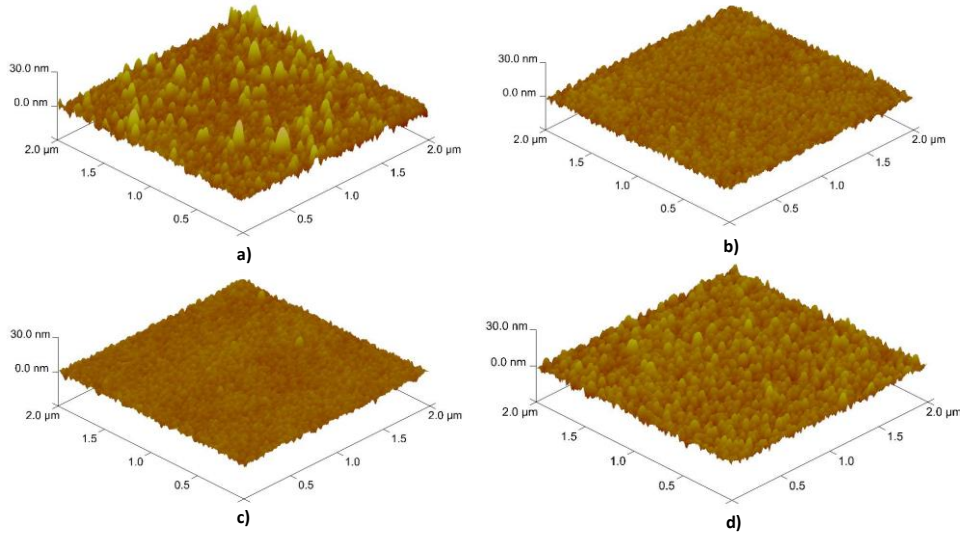
Figure 2. AFM scans of ZnO films at various temperatures; rms values: a) 125°C; 2.87 nm , b) 150°C; 1.82 nm, c)175°C; 1.4 nm, and d) 200°C; 2.62 nm. (ZnO filmleri AFM taraması pürüzlülük değerleri)

To find the size of the (100) and (002) grains, observed in XRD patterns and AFM images, the technique of X-ray line broadening was utilized. The Debye Scherrer equation $D(2\theta)=K\lambda/\ \beta\cdot\cos\theta$ was used to calculate the average grain sizes for (100) and (002) crystallites. Where D being the grain size, θ is the diffraction angle, λ the X-ray wavelength (λ= 1.5406 Ȧ), K represents the Scherrer constant (0.98) and β denotes the full width

at half max (FWHM) in radians. The crystallite sizes varied between 15-18 nm for (100) and 13-20 nm for (002) orientations depending on the growth condition. These values are in agreement with values obtained in literatıre [44]. As can be seen in Figure 3.c, with increase in temperature, both (100) and (002) crystallites grow larger. The (002) crystallites grow with higher rate due to high-temperature preferred Zn-rich growth mode
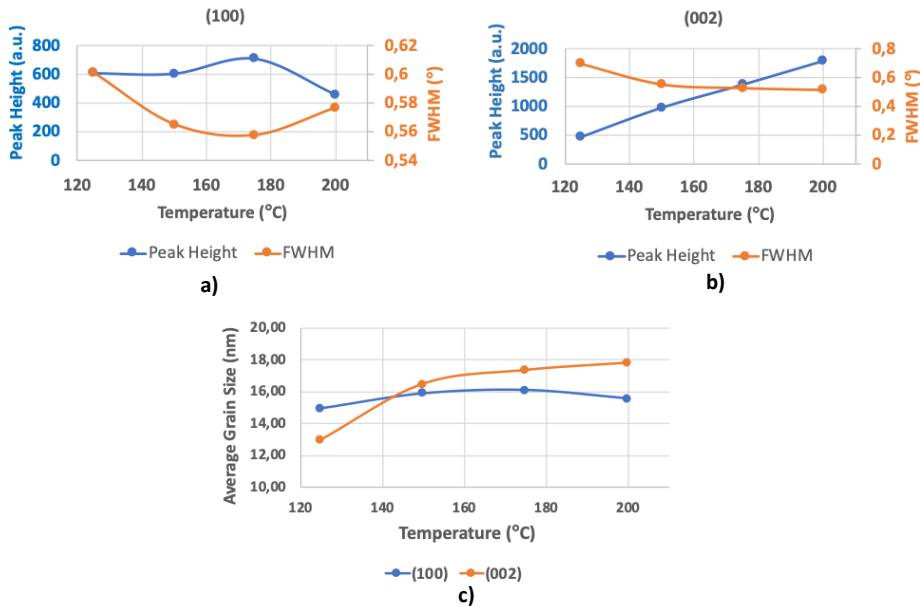
Figure 3. Effect of temperature on: **a)**(100) peak height and FWHM, **b)** (002) peak height and FWHM, and, **c)**(100) and (200) orientation grain size (Sıcaklığın a) (100) pik yüksekliğine ve FWHM'e, b) (002) pik yüksekliğine ve FWHM'e, c) (100) ve (200) oryantasyonunda tane büyüklüğüne etkisi)

To analyze the XRD and AFM results further, it is important to understand the surface reaction, adsorption and desorption dynamics well. When DEZ is pulsed on to a hydroxylated surface (with -OH group), one of the ethyl groups in DEZ takes the H atom from -OH group and purged out as ethane. This process leaves a surface oxygen attached to monoethyl zinc ligand (MEZ), the process followed with nitrogen purge and DI water pulse maintains the ALD growth cycle. Single MEZ-water exchange is low barrier (exothermic), however, MEZ saturated surface have a high ethyl-water exchange barrier. Therefore, adsorption of water with high MEZ covered Zn surface is inhibited by steric effect, so the growth favors (100). Some ethyl groups stay on surface even after DI water purge. Sufficiently long purge times and long DI water pulse times relative to DEZ pulse times creates higher ZnO formation, better stoichiometry and better surface features due to removal of ethyl ligands helping (002) growth. Similarly, short DI water purge leads to (100), and short DEZ pulse times favor (100) growth [42-43,31].
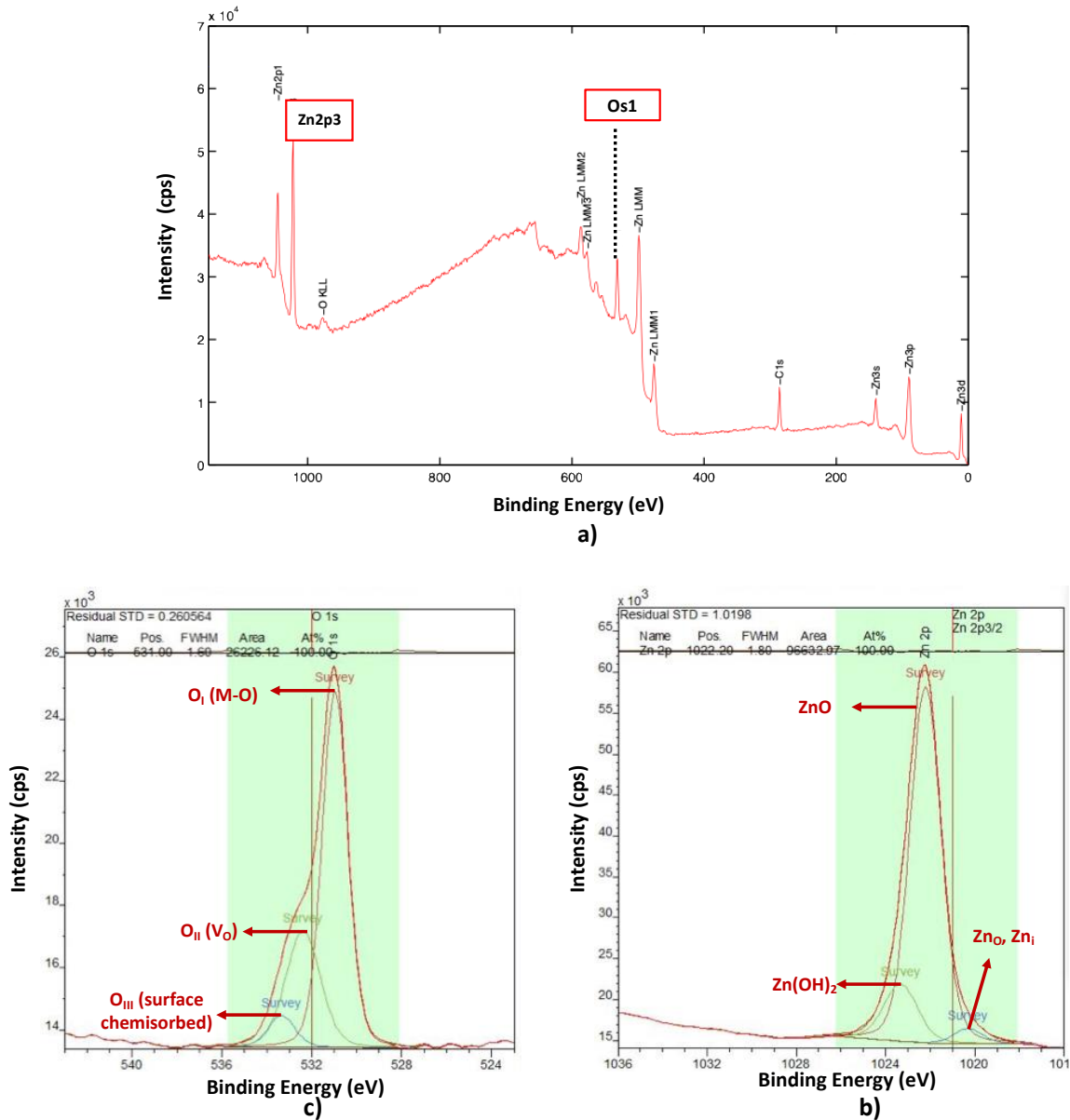
Figure 4. a) Representative XPS result for ZnO films, **b)**screenshot of CasaXPS analysis for O1s peak integrated binding energies distribution, and **c)** screenshot of CasaXPS analysis for Zn2p3/2 peak integrated binding energies distribution (a)ZnO filmler için temsili XPS sonucu, b) entegre bağlanma enerjileri dağılımından oluşan O1s pikinin CasaXPS analizi , c) entegre bağlanma enerjileri dağılımından oluşan Zn2p3/2 pikinin CasaXPS analizi)

As the DEZ and DI water pulse times increase (Group 2), surface roughness increases, and for increasing nitrogen purge times (Group 3), surface roughness decreases with a common reason: due to removal of ethyl ligands surface gets more saturated creating better stoichiometry ZnO formation with better surface features. Based on XRD scans, for Group 2, no significant change in (100) and (002) growth preference was observed for increasing purge time. And for the increasing DEZ/DI ratio (Group 4), XRD data shows (002) gets less intense up to ratio of 1 then the domination switches back to (002) crystallite formation. This trend is very similar to what was observed when increasing growth temperature (Group 1). The crystallites starts of with O-rich (100) orientation and it slowly switches back to Zn-rich (002) orientation. The decrease in surface roughness with increasing DEZ/DI ratio values also followed the same trend.

Stoichiometry: Point Defects and Impurities
(Stokiyometri: Noktasal kusurlar ve safsızlıklar)

O1s and Zn2p3/2 peaks were identified by XPS scan (Fig. 4.a). Each peak is composed of three Gaussian distribution revealing an information about the presence of each element (Zn or O) at different position and states. Using CasaXPS software each of these three distributions were identified. Accordingly, as depicted in Figure 4.b, O1s was compposed of O_I (centered at 530.5 eV) representing oxygen binded with metal (Zn), O_{II} (centered at 531.8 eV) representing oxygen deficiencies, and O_{III} (centered at 532.8 eV) representing oxygen chemisorbed on the surface with other species such as H_2O, O_2, CO_3, $Zn(OH)_2$ [26, 49, 50]. For Zn2p3/2 peak, as shown in Figure 4.c, the distribution centered around 1021.4 eV represents Zn metal (either interstitial or antisite, more likely being the interstitial due to lower formation energy), the state centered around 1022.3 eV representing ZnO, and the peak centered around 1023.2 eV belonging to $Zn(OH)_2$ [51, 52]. As an n-type conductivity mechanism oxygen vacancies, zinc interstitials and hydrogen impurities were considered as the probable n-type carriers. The relative formation energies, ionization energies and diffusion barriers were discussed previously in introduction. Therefore, ZnO (O_I) and oxygen vacancy-V_O (O_{II}) distributions were taken into consideration for electrical property analysis. O_{III} distribution was disregarded, as the peak represents more than one species (H_2O, O_2, CO_3, $Zn(OH)_2$) chemisorbed with hydrogen mostly on the surface. For Zn2p3/2 XPS peak, ZnO distribution, $Zn(OH)_2$ distribution (as representative of hydrogen carriers), and Zn metal distribution (as representative of zinc interstitials) were counted in the electrical analysis. All point defects and impurities (V_O, H, Zn_i) distributions were normalized with respect to measured ZnO distribution. The summary of % binding energy distribution of ZnO defects/impurities based on CasaXPS analysis is given in Table 5. The normalized oxygen vacancy area distribution from O1s, $Zn(OH)_2$ and Zn_i area distribution from Zn2p3/2 with respect to each ZnO area distribution are also given in the same table.

The dominant n-type carrier defects for Zn-rich ZnO films are oxygen vacancies and zinc interstitials. Oxygen vacancy concentration (V_O/ZnO) was increased, as the stoichiometry shifted toward zinc rich phase with increasing temperature. The Zn_i/ZnO ratio was much higher at 175°C compared to rest of the temperatures. The reason for Zn_i/ZnO ratio getting a sharp decrease at 200°C, has to do with interstitial Zn atoms diffusing out easily as the temperature gets higher. There was no significant effect of DEZn and DI water pulse times and of DEZn/DI ratio on V_O/ZnO. The V_O/ZnO was increased as the unreacted surface ligands pushed away and surface desorption rate increases with the increased purge time. The trends in Z_i was affected with growth dynamics that saturates stoichiometric Zn. As the Zn sites were saturated with O more, Zn_i formed less. In terms of hydrogen incorporation into the film, $Zn(OH)_2$/ZnO ratio did not change significantly with change in temperature. Increase in DEZn and DI water pulse times $Zn(OH)_2$/ZnO ratio, having more hydrogen incorporated in to film with increasing precursor pulse times due to increased rate of zinc oxygen combination. The more oxygen incorporated into films more hydrogen will be able to make bond with them. This is the same reason why $Zn(OH)_2$/ZnO ratio gets higher as the temperature is increased up to 175°C, but above this temperature oxygen will start to desorb from surface leaving less number of oxygen atoms to bond with hydrogen. Similar relationship discussion can be extended to increased DEZ/DI water ratio. Having these defects/impurities chemically incorporated into ZnO films does not necessarily mean that they are participating in the n-type conductivity. To figure out their role in conductivity, the normalized Hall resisitivity values will be correlated with the physical presence of these defects/impuritites to find a direct evidence.

Table 5. The % distribution of ZnO defects/impurities based on their binding energy levels calculated by CasaXPS from XPS measurements (XPS ölçümlerine dayanarak CasaXPS ile hesaplanan ZnO kusurları/safsızlıkları bağlanma enerjileri % dağılımı)

	Sample #	Variable sets	Variable	O_I area (M-O) (%)	O_{II} area (V_O) (%)	V_O/ZnO ratio	O_{III} area (surface chemisorbed) (%)	ZnO area (%)	$Zn(OH)_2$ area (%)	$Zn(OH)_2$/ZnO ratio	Zn ($Zn_{i,o}$) metal area (%)	$Zn_{i,o}$/ZnO ratio
GROUP 1	1	Increasing Temperature	200°C	55.7	30.83	0.55	13.47	87.06	12.14	0.14	0.79	0.01
	2		175°C	65.7	32.11	0.49	2.19	80.67	10.2	0.13	9.14	0.11
	3		150°C	62.16	31.97	0.51	5.86	80.33	13.49	0.17	6.18	0.08
	4		125°C	57.5	26.81	0.47	15.69	85.07	11.44	0.13	3.49	0.04
GROUP 2	5	Increasing DEZ & DI Pulse Time	100 ms	65.19	28.7	0.44	6.11	77.7	21.15	0.27	1.15	0.01
	6		50 ms	65.09	28.85	0.44	6.06	82.38	14.48	0.18	3.14	0.04
	2		15 ms	65.7	32.11	0.49	2.19	80.67	10.2	0.13	9.14	0.11
GROUP 3	6	Increasing Purge Time	10 s	65.09	28.85	0.44	6.06	82.38	14.48	0.18	3.14	0.04
	7		5 s	57.79	32.91	0.57	9.3	76.94	20.83	0.27	2.24	0.03
	8		2 s	63.83	29.97	0.47	6.2	84.13	14.85	0.18	1.02	0.01
GROUP 4	9	Increasing DEZ/DI Ratio	2	61.19	33.39	0.55	5.42	84.4	11.58	0.14	4.03	0.05
	5		1	65.19	28.7	0.44	6.11	77.7	21.15	0.27	1.15	0.01
	10		0.5	65.46	28.14	0.43	6.4	80.15	15.53	0.19	4.32	0.05
	11		0.25	65.56	28.73	0.44	5.71	79.13	15.05	0.19	5.81	0.07

Table 6. Summary of Hall measurement data and average % transmittance in the visible spectrum (380-700 nm) results (Hall ölçümü ve görünür bölgede ortalama % geçirgenlik değerleri)

	Sample #	Variable sets	Variable	Average Transmittance in Visible Range (380-700 nm)	Thickness on Quartz (nm)	Hall Resistivity (ohm.cm)	Carrier Density (/cm³)	Mobility (cm²/V.s)
GROUP 1	1	Increasing Temperature	200°C	74.3	73.61	0.047	1.23×10^{19}	10.82
	2		175°C	82.1	75.27	0.0074	3.43×10^{19}	24.5
	3		150°C	78.8	73.45	0.059	1.23×10^{19}	8.63
	4		125°C	75.6	64.3	NA	9.15×10^{13}	NA
GROUP 2	5	Increasing DEZ & DI Pulse Time	100 ms	86.5	78.08	0.0075	3.43×10^{19}	24.4
	6		50 ms	90	78.01	0.0068	4.79×10^{19}	19.17
	2		15 ms	82.1	75.27	0.0074	3.43×10^{19}	24.5
GROUP 3	6	Increasing Purge Time	10 s	90	78.01	0.0068	4.79×10^{19}	19.17
	7		5 s	92.3	80	0.0075	3.43×10^{19}	24.5
	8		2 s	82.1	82.1	0.0254	8.08×10^{19}	3.05
GROUP 4	9	Increasing DEZ/DI Ratio	2	89	79.75	0.0112	2.89×10^{19}	19.24
	5		1	86.5	78.08	0.0075	3.43×10^{19}	24.4
	10		0.5	79.8	78.78	0.0152	1.88×10^{19}	21.76
	11		0.25	76.3	78.65	0.0266	2.06×10^{19}	11.39

3.2. Electrical Properties (Elektriksel özellikler)

The summary of Hall measurements (Hall resistivity, carrier concentration and mobility) taken from ZnO films on quartz substrates utilizing Van der Pauw pattern at room temperature; thickness of ZnO films on quartz substrate; and average % transmittance measured in visible spectrum (380-700 nm) are given in Table 6. The c-[0001] direction grown polar (002) planes have higher bandgap (3.37 eV) than perpendicular non-polar (001) planes, and it contributes to conductivity more than (001) planes.

Mobility and carrier densities increased and so the resistivity values decreased with increase in growth temperature. DEZ and DI water pulse times, varying nitrogen pulse times did not affect the resistivity

values subtantially. The lowest resistivity value was obtained at 175°C as 0.0074 ohm.cm. Resistivities were lowest at all purge times, DEZ/DI ratio of 1, and all DEZ and DI water pulse times. The carrier densities ranged in between $1-8 \times 10^{19}$ /cm^3, and the mobility values were 3-24.5 cm^2/Vs. These carrier density, moblity and resistivity values are compatible with highest literature values [53,54].

Electrical Property-Structural Property Dynamics
(Elektriksel özellik-yapısal özellik dinamikleri)

The effect of zero dimensional defect/impurity concentrations on resistivity values were investigated to see which candidate defect/impurity makes contribution to n-type conduction. The physical presence of these defects/impurities were measured by XPS and alayzed with CasaXPS. However, if their ionization energies are high or if they are compensated, there would not be any contribution to conductivity.

All defect types (including grain boundaries, dislocations) and impurities are the factors affecting the resistivity values. Grain boundaries act like scattering centers for free carriers. These boundaries are also the source of dislocations and accumulation centers for n-type ZnO compensator zinc vacancies. So there is a strong correlation in between the size of the grains and resistivity. Zinc vacancies concentration increases with increase in grain boundary area, so increase in resistivity with grain size reduction is observed for all experiment groups.

Table 7. The summary of relative amounts of normalized ZnO defects, weighted average grain size of (100) and (002) peaks, and their effect on normalized resistivity data (ZnO kusurlarının, (100) ve (002) tanelerinin ağırlıklı ortalaması alınan tane boyutunun ve özdirencin normalize edilmiş değerleri)

	Sample #	Variable sets	Variable	V_O/ZnO ratio	$Zn(OH)_2$/ZnO ratio	$Zn_{i,O}$/ZnO ratio	Weighted average grain size (nm)	Normalized resistivity
GROUP 1	1	Increasing Temperature	200°C	0.55	0.14	0.01	17.36	0.8158
	2		175°C	0.49	0.13	0.11	16.94	0.1254
	3		150°C	0.51	0.17	0.08	16.27	0.9601
	4		125°C	0.47	0.13	0.04	14.13	NA
GROUP 2	5	Increasing DEZ & DI Pulse Time	100 ms	0.44	0.27	0.01	16.54	0.1241
	6		50 ms	0.44	0.18	0.04	14.66	0.0997
	2		15 ms	0.49	0.13	0.11	16.94	0.1254
GROUP 3	6	Increasing Purge Time	10 s	0.44	0.18	0.04	14.66	0.0997
	7		5 s	0.57	0.27	0.03	15.48	0.1161
	8		2 s	0.47	0.18	0.01	15.19	0.3859
GROUP 4	9	Increasing DEZ/DI Ratio	2	0.55	0.14	0.05	18.18	0.2036
	5		1	0.44	0.27	0.01	16.54	0.1241
	10		0.5	0.43	0.19	0.05	17.08	0.2596
	11		0.25	0.44	0.19	0.07	19.15	0.5094

The average crystalite sizes can be correlated to change in electrical behaviour for polycrystalline ZnO films due to the grain boundary scattering and dislocation effect on free carriers. The crystallite size also can be related with dislocation density [45-48], as the dislocations are located on the grain boundaries. Smaller the grains larger the grain boundaries, so higher number of dislocations. Therefore, the calculated average grain sizes for (100) and (002) crystallites were utilized in combination with (100) and (002) relative XRD peak intensities to obtain a weighted average grain size (WAGS) of ZnO films for each growth condition. Therefore, to single out the effect of grain boundary potential barrier effect on resistivity values, all Hall resistivity values were normalized with respect to the calculated WAGS. Mathematically, these WAGS values were multiplied by Hall resistivity values to obtain normalized resistivity values. So that an anlysis in between point defects/impurities and resistivity can be carried out while ruling out the other defect effects.

The values obtained as a result of these calculations are presented in Table 7. The change in each specific candidate defect/impurity level and normalized resistivity values were plotted against each varying growth condition in Figure 5 (for Group 1), Figure 6 (for Group 2), Figure 7 (for Group 3) and Figure 8 (Group 4). To have a certain defect contribution, the evidence should suggest inverse relationship between the change in certain defect/impurity type concentation versus resistivity, i.e. if a certain defect concentration increases, the resistivity values should decrease with it. Although, there was no strong correlation for oxygen vacancies, the contribution of hydrogen impurities, zinc interstitals and oxygen vacancies to conductivity was observed at different growth conditions. The data sets that were a direct evidence of inverse relationship between the changes in defect/impurity concentration and resistivity are: Zn interstitial at varying temperatures, OH/ZnO (hydrogen impuritiy) at varying DEZn/DI water ratio, and all types of defect/impurities when purge time was varied, especially up to 5 seconds.

Playing with DEZn/DI ratio to obtain a balanced ZnO stoichiometry at sufficiently long purge times (more than 5 second) and sufficiently high growth temperatures in ALD growth window yields hydrogen carrier dominated lowest resistivity values. Figure 6 suggests, to obtain a meaningful relationship between resistivity and defect/impurity contributions, DEZn and DI water pulse times should be at least 50 ms and more. The surface saturation can be accomplished at sufficiently long pulse times.

Zinc interstitial contribution to conductivity at changing growth temperatures was observed. As the temperature increased ZnO films gets Zn rich and some of the Zn atoms takes the interstitial sites, known to be a shallow donor. The number of Zn interstitials increase up to 175°C, then decreases dramatically at 200°C. Most likely increased chances of Zn atoms diffusing out of interstitial sites. The dramatic decrease in Zn interstitials also translated into dramatic increase in resistivities (Figure 5.c). This strong correlation suggests depending on the growth temperature zinc interstitials can be a contributor to n-type conductivity.
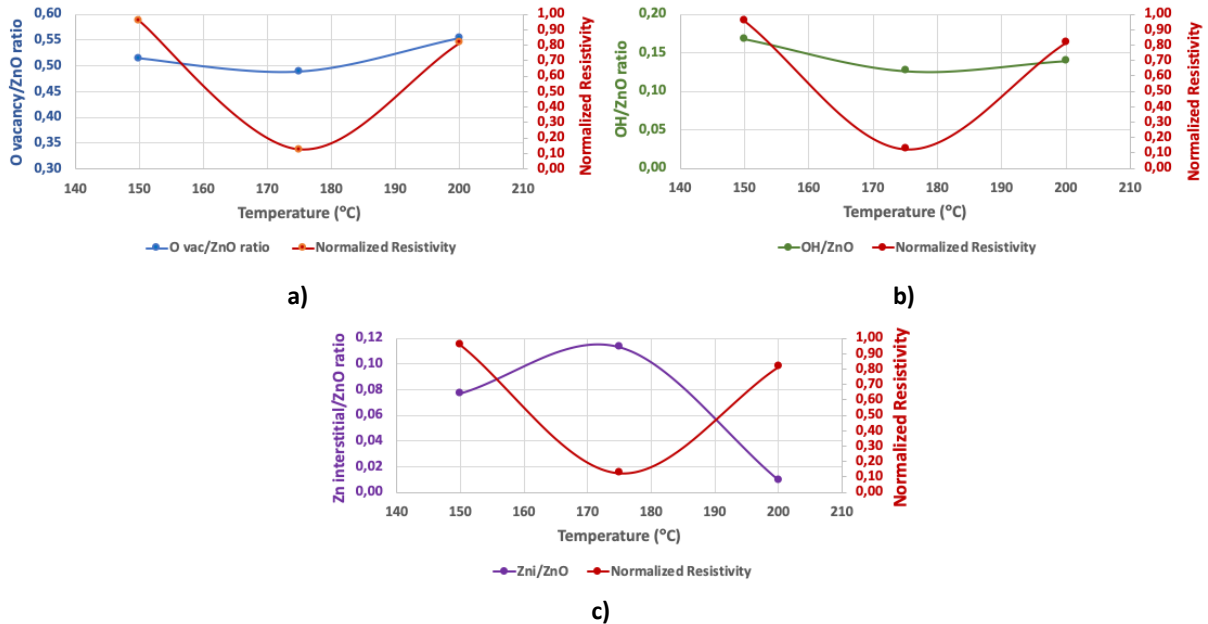
Figure 5. The effect of growth temperature on **a)** normalized concentration of V_O and its correlation with normalized resistivity, **b)** normalized concentration of OH and its correlation with normalized resistivity, **c)** normalized concentration of Zn_i and its correlation with normalized resistivity. (Büyüme sıcaklığının, a) normalize edilmiş oksijen boşlukları konsantrasyonu ve normalize edilmiş özdirenç ilişkisine, b) normalize edilmiş OH konsantrasyonu ve normalize edilmiş özdirenç ilişkisine, c) normalize edilmiş atomlar arası çinko konsantrasyonu ve normalize edilmiş özdirenç ilişkisine etkileri)
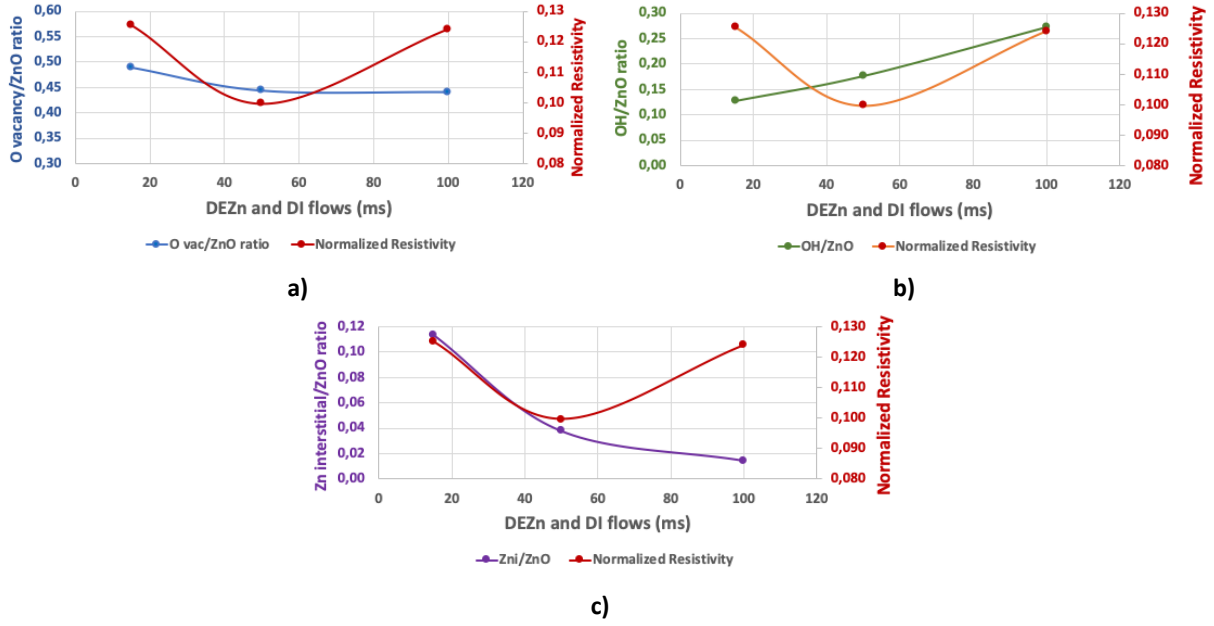
Figure 6. The effect of DEZ and DI water pulse times (at DEZ/DI ratio=1) on **a)** normalized concentration of V_O and its correlation with normalized resistivity, **b)** normalized concentration of OH and its correlation with normalized resistivity, **c)** normalized concentration of Zn_i and its correlation with normalized resistivity. (DEZ ve DI atış sürelerinin (DEZ/DI oranı sabit olarak 1 iken), a) normalize edilmiş oksijen boşlukları konsantrasyonu ve normalize edilmiş özdirenç ilişkisine, b) normalize edilmiş OH konsantrasyonu ve normalize edilmiş özdirenç ilişkisine, c) normalize edilmiş atomlar arası çinko konsantrasyonu ve normalize edilmiş özdirenç ilişkisine etkileri)
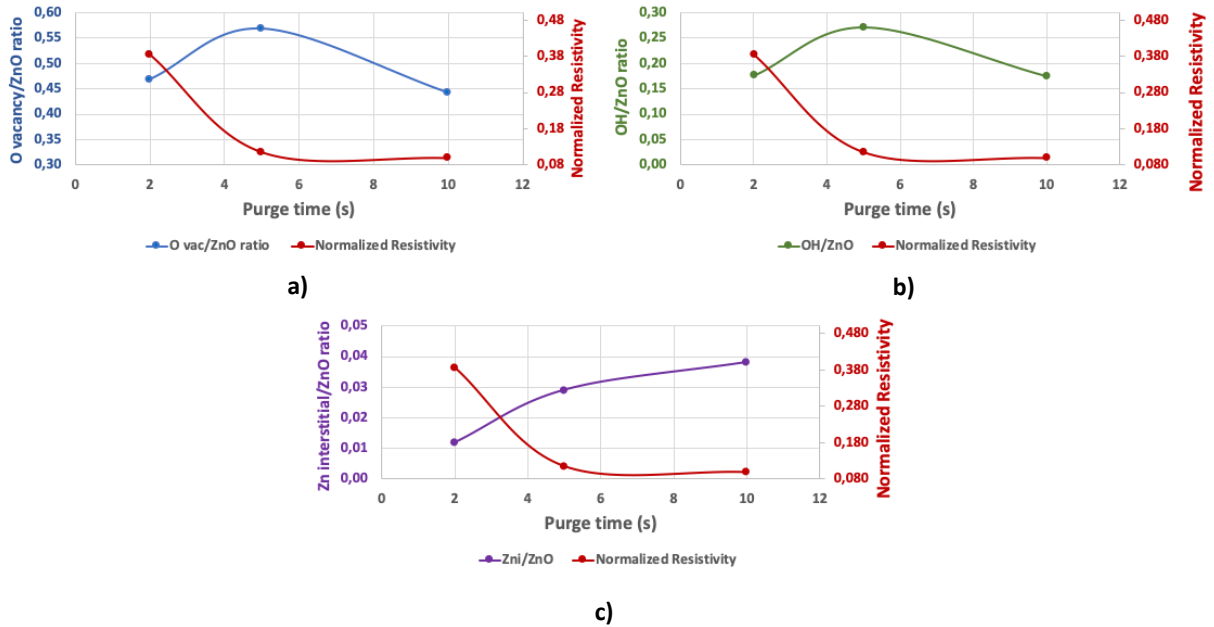
Figure 7. The effect of nitrogen purge time on **a)** normalized concentration of V_O and its correlation with normalized resistivity, **b)** normalized concentration of OH and its correlation with normalized resistivity, **c)** normalized concentration of Zn_i and its correlation with normalized resistivity. (Azot yıkama süresinin, a) normalize edilmiş oksijen boşlukları konsantrasyonu ve normalize edilmiş özdirenç ilişkisine, b) normalize edilmiş OH konsantrasyonu ve normalize edilmiş özdirenç ilişkisine, c) normalize edilmiş atomlar arası çinko konsantrasyonu ve normalize edilmiş özdirenç ilişkisine etkileri)
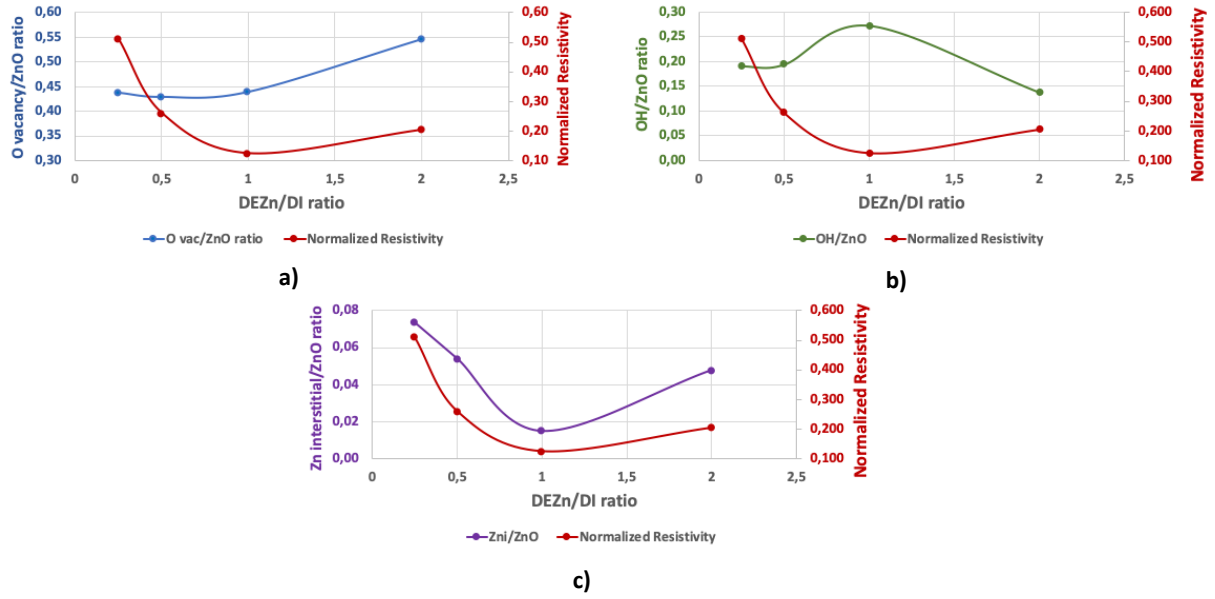
Figure 8. The effect of DEZ/DI ratio on **a)** normalized concentration of V_O and its correlation with normalized resistivity, **b)** normalized concentration of OH and its correlation with normalized resistivity, **c)** normalized concentration of Zn_i and its correlation with normalized resistivity. (DEZ/DI oranının, a) normalize edilmiş oksijen boşlukları konsantrasyonu ve normalize edilmiş özdirenç ilişkisine, b) normalize edilmiş OH konsantrasyonu ve normalize edilmiş özdirenç ilişkisine, c) normalize edilmiş atomlar arası çinko konsantrasyonu ve normalize edilmiş özdirenç ilişkisine etkileri)

The strongest correlation was observed for hydrogen (as $Zn(OH)_2$) at varying DEZn/DI water ratios. After temperature, the most influential growth parameter on structural properties was DEZn/DI water pulse time ratio. At 175°C growth temperature and 10 second purge time, as DEZn/DI ratio was increased (50/200, 50/100, 100/100) from 0.25 to 1, ZnO films went from O-rich to Zn-rich. At the ratio of 1 the lowest resistivities were obtained along with highest hydrogen concentration as can be seen in Figure 8.b. The 100/100 ratio led to saturated Zn sites and stoichiometrically balanced ZnO films. XRD data also suggested a balanced mix between (100) and (002) orientations. After DEZn/DI ratio of 2, XRD data and XPS data suggested that ZnO films are in Zn-rich/O-defficient with increased oxygen vacancies. Therefore, the number of hydrogens existed as attached to OH decreased and the resistivity values increased. This is a strong direct evidence that hydrogen impurities are the main contributors to n-type conductivity in ZnO. There was no correlation between the oxygen vacancy concentration nor zinc interstitials, and resistivities for change in DEZn/DI ratio.
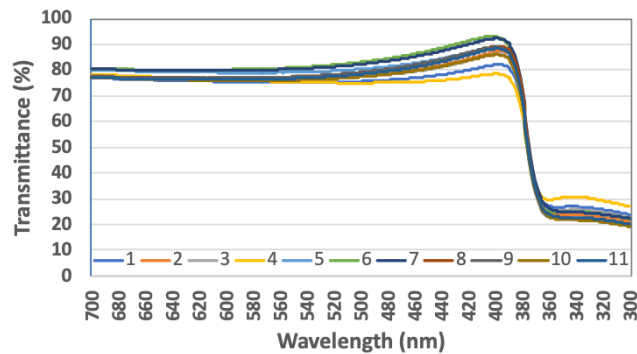
Figure 9. % Transmittance in visible spectrum of 11 samples with various ALD growth parameters (Farklı ALD büyütme parametreleri ile büyütülmüş 11 numunenin görünür bölgede % geçirgenliği)

3.3. Optical Property: %Transmittance
(Optik özellikler: % Geçirgenlik)

In addition to electrical properties, average % transmittance values in visible wavelength range was taken as shown in Figure 9 and Table 6. Accordingly, these values ranged from 74.3% for 200°C grown sample to 92.3% for 5 second nitrogen purged sample. The same values ranged from 74% to 90% in literature [55]. Therefore the data obtained in this work is in agreement with literature data and can be used for TCO applications.

4. CONCLUSIONS (SONUÇLAR)

The influence of different type of defects and impurities on the electrical behaviour of ZnO has long been debated. DFT calculations theoretically suggested hydrogen is the main carrier for n-type conductivity in ZnO [7,25-26, 28-31]. While many experimental researchers suggested oxygen vacancies or the zinc interstitials as the source of n-type conductivity [32-35]. In this study, these defect/impurity formations based on growth conditions and their contribution to electrical conductivity was expermentally investigated.

According to structural studies, the most important growth parameter that controls the surface reaction dynamics was temperature. The second most important parameter was DEZ to DI ratio. Once the purge time was kept at sufficiently long times (5 sec and above) and the DEZ and DI water pulse times kept at sufficiently long times to saturate the surface (50 ms and above), playing with gorwth temperature and tuning in the DEZ/DI ratio would give the lowest resistivity values. There was a strong evidence that hydrogen impurities in the form of $Zn(OH)_2$ contributes to n-type conductivity. Another correlation suggested depending on the growth temperature zinc interstitials can be a contributor to n-type conductivity. This correlation should be investigated for longer (50 ms and longer) DEZ and DI water pulse times. There was a little evidence that oxygen vacancies can be a contributor to n-type conductivity in ZnO films.

The lowest resistivity value was obtained at 175°C as 0.0074 ohm.cm. The carrier densities ranged in between $1-8\times10^{19}$ /cm^3, and the mobility values were 3-24.5 cm^2/Vs. The highest average % transmittance value obtained was 92.3%.

DECLARATION OF ETHICAL STANDARDS
(ETİK STANDARTLARIN BEYANI)

The author of this article declares that the materials and methods they use in their work do not require ethical committee approval and/or legal-specific permission.

Bu makalenin yazarı çalışmalarında kullandıkları materyal ve yöntemlerin etik kurul izni ve/veya yasal-özel bir izin gerektirmediğini beyan ederler.

AUTHORS' CONTRIBUTIONS (YAZARLARIN KATKILARI)

Bilge İMER: She conducted the experiments, analyzed the results and performed the writing process.

Deneyleri yapmış, sonuçlarını analiz etmiş ve maklenin yazım işlemini gerçekleştirmiştir.

CONFLICT OF INTEREST (ÇIKAR ÇATIŞMASI)

There is no conflict of interest in this study.

Bu çalışmada herhangi bir çıkar çatışması yoktur.

REFERENCES (KAYNAKLAR)

[1] Salami, H., Uy, A., Vadapalli, A., Grob, C., Dwivedi, V., & Adomaitis, R. A., Atomic layer deposition of ultrathin indium oxide and indium tin oxide films using a trimethylindium, tetrakis(dimethylamino)tin, and ozone precursor system, Journal of Vacuum Science & Technology A: Vacuum, Surfaces, and Films, 37(010905), (2019).

[2] Frank, G., and Köstlin, H., Electrical properties and defect model of tin-doped indium oxide layers, Applied Physics A Solids and Surfaces, 27(4) (197–206), (1982).

[3] Choi, Y. J., and Park, H. H., A simple approach to the fabrication of fluorine-doped zinc oxide thin films by atomic layer deposition at low temperatures and an investigation into the growth mode, Journal of Materials Chemistry C, 2(1) (98–108), (2014).

[4] Khan, S., & Stamate, E., Comparative Study of Aluminum-Doped Zinc Oxide, Gallium-Doped Zinc Oxide and Indium-Doped Tin Oxide Thin Films Deposited by

Radio Frequency Magnetron Sputtering, Nanomaterials, 12(9), (2022).

[5] Polat Gonullu, M., and Ates, H., An Overview of Atomic Layer Deposition Technique: Synthesis of ZnO, TiO₂ and Al₂O₃ Films, GU J Sci, Part C, 7(3) (649-660), (2019).

[6] Florescu, D.I., Mourokh, L.G., Pollak F.H., Look, D.C., Cantwell, G., and Li, X., High spatial resolution thermal conductivity of bulk ZnO (001), Journal of Applied Physics, 91 (890-892), (2002).

[7] Ozgur, U., Alivov, I., Liu, C., Teke, A., Reshchikov, M.A., Dogan, S., Avrutin, V., Cho, S.J., and Morkoc, H., A comprehensive review of ZnO materials and devices, Journal of Applied Physics, 98 (041301), (2005).

[8] Tuomisto, F., Saarinen, K., Look, D.C., and Farlow, G.C., Physical Review B, 72 (085206), (2005).

[9] Mang, A., Reimann, K., and Rübenacke, S., Bandgaps, crystal-field splitting, spin-orbit coupling, and exciton binding energies in ZnO under hydrostatic pressure, Solid State Communications, 94 (4) (251-254), (1995).

[10] Reynolds, D.C., Look, D.C., and Jogai, B., Optically Pumped Ultraviolet Lasing From ZnO, Solid State Communications, 99 (12) (873-875), (1996).

[11] Molarius, J., Kaitila, J., Pensala, T., Ylilammi, M., Piezoelectric ZnO films by r.f. sputtering, J. Of Matr. SCİ.: MATERİALS İN ELECTRONİCS, 14 (431-435), (2003).

[12] Look, D.C., Recent advances in ZnO materials and devices. Mater Sci Eng B., 80 (383-387), (2001).

[13] Nause, J. and Nemeth, B., Pressurized melt growth of ZnO boules, Semiconductor Science and TECHNOLOGY, 20(4) (S45-S48), (2005).

[14] Klingshirn, C., ZnO: From basics towards applications, Physica Status Solidi (b), 244(9) (3019-3407), (2007).

[15] Ellmer, K., Past achievements and future challenges in the development of optically transparent electrodes, Nature Photonics, 6 (809-817), (2012).

[16] Pearton, S., and Ren, F., Advances in ZnO-based materials for light emitting diodes, Current Opinion in Chemical Engineering, 3 (51-55), (2014).

[17] Hultqvist, A., Aitola, K., Sveinbjörnsson, K., Saki, Z., Larsson, F., Törndahl, T., Johansson, E., Boschloo, G., Edoff, M., Atomic Layer Deposition of Electron Selective SnO x and ZnO Films on Mixed Halide Perovskite: Compatibility and Performance. ACS applied materials & interfaces, 9 (29707-29716), (2017).

[18] Carcia, P.F., McLean, R.S., and Reilly, M.H., High-performance ZnO thin-film transistors on gate dielectrics grown by atomic layer deposition, Applied Physics Letters, 88 (123509), (2006).

[19] Ye, Z., Xu, H., Liu, T., Liu, N., Wang, Y., Zhang, N., and Liu, Y., Highly Stable Atomic Layer Deposited Zinc Oxide Thin-Film Transistors Incorporating Triple O₂ Annealing, IEEE Transactions on Electronic Devices, 64-10 (4114-4122), (2017).

[20] Karpina, V., Lazorenko, V., Lashkarev, C., Dobrowolski, V., Kopylova, L., Baturin, V., Pustovoytov, S., Karpenko, A. J., Eremin, S., and Lytvyn, P., Zinc oxide–analogue of GaN with new perspective possibilities, Crystal Research and Technology, 39 (980-992), (2004).

[21] Gorla, C., Emanetoglu, N., Liang, S., Mayo, W., Lu, Y., Wraback, M., and Shen, H., Structural, optical, and surface acoustic wave properties of epitaxial ZnO films grown on (0112) sapphire by metalorganic chemical vapor deposition, J. Appl. Phys., 85 (2595-2602), (1999).

[22] Jung, S., Park, W., Cheong, H., Yi, G.C., Jang, H., Hong, S., and Joo, T., Time-resolved and time-integrated photoluminescence in ZnO epilayers grown on Al₂O₃ (0001) by metalorganic vapor phase epitaxy, Applied Physics Letters, 80 (1924), (2002).

[23] Zu P., Tang, Z.K, Wang, G.K.L., Kawasaki, M., Ohtomo, A., Koinuma, H.,

and Segawa, Y., Solid State Communications, 103 (459-463), (1997).

[24] Jin, B.J.,Im, S., and Lee, S.Y., Violet and UV luminescence emitted from ZnO thin films grown on sapphire by pulsed laser deposition, Thin Solid Films, 366 (107-110), (2000).

[25] Janotti, A., and Van De Walle, C.G., Fundamentals of zinc oxide as a semiconductor, Reports on Progress in Physics, 72 (126501), (2009).

[26] Ayoub, I., Kumar, V., Abdolhassani, R., Sehgal, R., Sharma, V., Sehgal, R, Swart, H.C., and Mishra, Y.K., Advances in ZnO manipulation of defects for enhancing their technological potentials, Nanotechnology Reviews, 11 (575-619), (2022).

[27] Dutta, S, Chattopadhyay, S., Sarkar, A., Chakrabarti, M., Sanyal, D., and Jana D., Role of defects in tailoring structural, electrical and optical properties of ZnO, Progress in Materials Science, 54 (89-136), (2009).

[28] Janotti, A., and Van De Walle, C.G., Oxygen vacancies in ZnO, Applied Physics Letters, 87 (122102), (2005).

[29] Janotti, A., and Van de Walle, C.G., New insights into the role of native point defects in ZnO, Journal of Crystal Growth, 287 (58–65), (2006).

[30] Janotti, A., and Van de Walle, C.G., Native point defects in ZnO, Phys Rev B., 76 (165202), (2007).

[31] Guziewicz, E., Godlewski, M., Krajewski, T.A., Wachnicki, L., Luka, G., Domagala, J.Z., Paszkowicz, W., Kowalski,B.J., Witkowski, B.S., Duzynska, A., and Suchocki, A., Zinc oxide grown by atomic layer deposition - a material for novel 3D electronics, Physica Status Solidi (b) 247 (1611-1615), (2010).

[32] Liu, L., Mei, Z., Tang, A., Azarov, A., Kuznetsov, A., Xue, Q., and Du, X., Oxygen vacancies: The origin of n-typeconductivity in ZnO, Physical Review B, 93 (235305), (2016).

[33] Halliburton, L.E., Giles, N.C., Garces, N.Y., Luo, M., Xu, C., Bai, L. and Boatner, L.A., Production of native donors in ZnO by annealing at high temperature in Zn vapor, Applied Physics Letters, 87 (172108), (2005).

[34] Hagemark, K.I., and Toren, P.E., Determination of Excess Zn in ZnO: The Phase Boundary. Journal of Electrochemical Society, 122 (992), (1975).

[35] Tuomisto, F., Saarinen, K., Grasza, K., and Mycielski, A., Observation of Zn vacancies in ZnO grown by chemical vapor transport, Physica Status Solidi (b), 243(4) (794-798), (2006).

[36] Guziewicz, E., Krajewski, T.A., Przezdziecka, E., Korona, K.P., Czechowski, N., Klopotowski, L., and Terziyska, P., Zinc Oxide Grown by Atomic Layer Deposition: From Heavily n-Type to p-Type Material, Phys. Status Solidi B, 257 (1900472), (2020).

[37] Guziewicz, E., Godlewski, M., Wachnicki, L., Krajewski, T.A., Luka, G., Gieraltowska, S., Jakiela, R., Stonert, A., Lisowski, W., Krawczyk, M., Sobczak, J.W., and Jablonski, A., Semiconductor Science and Technology, 27 (074011), (2012).

[38] Guziewicz, E., Kowalik, I.A., Godlewski, M., Kopalko, K., Osinniy, V., Wojcik, A., Yatsunenko, S., Lusakowska, E., Paszkowicz, W., and Guziewicz, M., Extremely low temperature growth of ZnO by atomic layer deposition, Journal of Applied Physics, 103 (033515), (2008).

[39] Pung, S., Choy, K., Hou, X., and Shan, C., Preferential growth of ZnO thin films by the atomic layer deposition technique, Nanotechnology, 19 (435609), (2008).

[40] Weckman, T., and Laasonen, K., Atomic Layer Deposition of Zinc Oxide: Study on the Water Pulse Reactions from First-Principles, The Journal of Physical Chemistry, 122 (7685-7694), (2018).

[41] Fujimura, N., Nishihara, T., Goto, S., Xu, J., and Ito, T., Control of preferred orientation for ZnOx films: control of self-

texture, Journal of Crystal Growth, 130 (269-279), (1993).

[42] Nguyen, T.,Valle, N., Guillot, J., Bour, J., Adjeroud, N., Fleming, Y., Guennou, M., Audinot, J.N., El Adib, B., Joly, R., Arl, D., Frache, G., and Polesel-Maris, J., Elucidating the growth mechanism of ZnO films by atomic layer deposition with oxygen gas via isotopic tracking, Journal of Materials Chemistry C, 9 (4307-4315), (2021).

[43] Lim, J., and Lee, C., Effect of substrate temperature on the microstructure and photoluminescence properties of ZnO thin films prepared by atomic layer deposition, Thin Solid Films, 515 (3335-3338), (2007).

[44] Cabral, L., Lopez-Richard, V., Da Silva, J.L.F., Marques, G.E., Lima, M.P., Onofre, Y.J., Teodoro, M.D., and Godoy, M.P.F., Insights into the nature of optically active defects of ZnO, Journal of Luminescence, 227 (117536), (2020).

[45] Iqbal, J., Jilani, A., Hassan, P.M.Z., Rafique, S., Jafer, R., and Alghamdi, A.A., ALD grown nanostructured ZnO thin films: Effect of substrate temperature on thickness and energy band gap, Journal of King Saud Universiyt-Science, 28 (347-354), (2016).

[46] Gordillo, G., Florez, J.M., and Hernandez, L.C., Preparation and characterization of CdTe thin films deposited by CSS, Solar Energy Materials and Solar Cells, 37 (273-281), (1995).

[47] Ameur, S.B., Bel hadjltaief, H., Barhoumi, A., Duponchel, B., Leroy, G., Amlouk, M., and Guermazi, H., Physical investigations and photocatalytic activities on ZnO and SnO2 thin films deposited on flexible polymer substrate, Vacuum, 155 (546-552), (2018).

[48] Mishra, S., Przezdziecka, E., Wozniak, W., Adhikari, A., Jakiel, R., Paszkowicz, W., Sulich, A., Ozga, M., Kopalko, K., and Guziewicz, E., Structural Properties of Thin ZnO Films Deposited by ALD under O-Rich and Zn-Rich Growth Conditions and Their Relationship with Electrical Parameters, Materials, 14 (4048), (2021).

[49] Jain, S., Shah, J., Negi, N.S., Sharma, C., and Kotnala, R.K., Significance of interface barrier at electrode of hematite hydroelectric cell for generating ecopower by water splitting, International Journal of Energy Research, 44, 14 (11111-11134), (2019).

[50] Cho, Y., and Kang, K., and Park, H., Anion-controlled passivation effect of the atomic layer deposited ZnO films by F substitution to O-related defects on the electronic band structure for transparent contact layer of solar cell applications, Solar Energy Materials & Solar Cells, 132 (403-409), (2015).

[51] Crist B.V., (1999) Handbook of Monochromatic Xps Spectra, vol. 2, Commercially Pure Binary Oxides, XPS International Inc., Mountain View, California, 94040, USA, (818-827).

[52] Galmiz, O., Stupavska, M., Wulff, H., Kersten, H., Brablec, A., Cernak, M., Deposition of Zn-containing films using atmospheric pressure plasma jet, Open Chem., 13 (198-203), (2015).

[53] Godlewski, M., Guziewicz, E., Luka, G., Krajewski, T., Lukasiewicz, M., Wachnicki, L., Wachnicka, A., Kopalko, K., and Dalati, A.S., ZnO layers grown by Atomic Layer Deposition: A new material for transparent conductive oxide, Thin Solid Films, 518 (1145-1148), (2009).

[54] Chandrasekar, L.B., Nagarajan, S., Karunakaran, M., and Thangadurai, T.D., (2019) Structural, optical and electrical properties of undoped and doped ZnO thin films, 2D Materials, eBook.

[55] Laube, J., Nübling, D., Ben, H., Gutsch, S., Hiller, D., and Zacharias, M., Resistivity of atomic layer deposition grown ZnO: The influence of deposition temperature and post-annealing, Thin Solid Films, 603 (377-381), (2016).